General Disclaimer

One or more of the Following Statements may affect this Document

- This document has been reproduced from the best copy furnished by the organizational source. It is being released in the interest of making available as much information as possible.

- This document may contain data, which exceeds the sheet parameters. It was furnished in this condition by the organizational source and is the best copy available.

- This document may contain tone-on-tone or color graphs, charts and/or pictures, which have been reproduced in black and white.

- This document is paginated as submitted by the original source.

- Portions of this document are not fully legible due to the historical nature of some of the material. However, it is the best reproduction available from the original submission.

NASA Contractor Report 156848

On the Determination and Investigation of the Terrestrial Ionospheric Refractive Indices Using GEOS-3/ATS-6 Satellite-to-Satellite Tracking Data

Anthony S. Liu

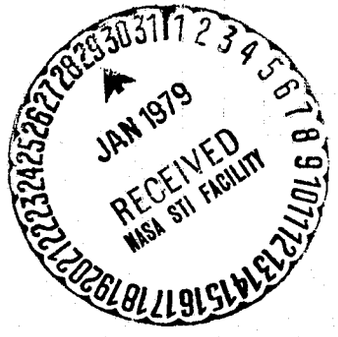

November 1978

National Aeronautics and Space Administration

Wallops Flight Center
Wallops Island, Virginia 23337
AC 804 824-3411

INTRODUCTION

During 1974 and 1975, two Earth satellites were placed into orbit. The first was the Applications Technology Satellite (ATS-6). It is equipped with a wide variety of radio communication capabilities. This satellite is in a geostationary orbit and during the time of this experiment was located over 94°W longitude. The second satellite was the Geodynamics Experimental Ocean Satellite (GEOS-3). It is equipped with a wide range of geodetic and oceanographic sensing devices, and is capable of communicating at S-band (about 2×10^3 MHz).

The ATS-6 spacecraft has a phase coherent frequency translator which enables ATS-6 to shift the ground reference frequency from C-band (about 6×10^3 MHz) to S-band, thereby linking up with GEOS-3. This S-band radio link between GEOS-3 and ATS-6 provides the Satellite-to-Satellite Tracking (SST) data.

GEOS-3 is in a circular polar orbit, inclined at 115° at an altitude of 800 km. Once every GEOS-3 orbital period of 100 min, GEOS-3 disappears (occults) behind the Earth, as seen from ATS-6. Since the Earth to ATS-6 line turns underneath the GEOS orbital plane, occultations occur at maximum northerly and southerly latitudes of 65° when the GEOS-3 orbit plane is edgewise to ATS-6. Nearly equatorial occultations occur when the GEOS-3 orbit plane is normal to ATS-6.

The effect of the intervention of the atmosphere upon the SST signal, during occultation, is two-fold. First, because the signal travels through an atmosphere with a non-unity refractive index, the phase of the Doppler signal is retarded in the neutral portion and advanced in the ionosphere part of the atmosphere. Secondly, the path of the signal is bent, and therefore lengthened. The combination of these two effects causes apparent increase in the radio path length between GEOS-3 and ATS-6 for the neutral atmosphere, but an apparent decrease as the signal penetrates the ionosphere portion of the atmosphere. Thus, as GEOS-3 disappears behind the Earth, the

ATS-6/GEOS-3 Doppler residuals will show first a shortening of the phase path when the signal traverses through the upper plasma regions, then a null region, and eventually, when the signal pierces the thicker portions of the neutral gas, the phase path will be lengthened from that of free space. This sequence occurs twice per GEOS-3 pass as seen by ATS-6: once on entrance into occultation (immersion) and again upon exit as GEOS-3 reappears from behind the Earth (emersion). Since ATS-6 is geostationary, occultations occur at latitudes between $\pm$ 65°, over a 12 hr period.

The SST data link provides a unique geometrical aspect to the terrestrial atmosphere. A lateral picture at various altitudes of the Earth's atmosphere and ionosphere is obtained not only at the near north and south polar regions ($\pm$ 65° latitude) but also at many intermediate latitudes.

In contrast to vertical sounding methods used earlier, the SST data gives a horizontal picture of the ionosphere. If one assumes spherical symmetry one can get an entire altitude profile without resorting to merging data from bottom radiosounds and topside rocket measurements.

The probing of an atmosphere by a coherent radio frequency is not new. This present investigation is a terrestrial application of those techniques used to analyze the Martian ionosphere and atmosphere [A. Kliore, D. Cain, G. S. Levy, V. R. Eshleman, G. Fjeldbo, F. Drake, 1965]. Numerous investigators used the occultation of two Earth satellites to study the terrestrial atmosphere. An investigation of the application of microwave occultations between two Earth satellites for meteorological data was made by Morrison, Ungar, and Lusignan [1972]. Kliore [1969] considered using this occultation method for monitoring weather disturbances. A dual frequency link between Apollo and Soyuz to measure the horizontal electron content was proposed by Grossi and Gay [1975]. The measurements and analysis from the Apollo-Soyuz data were reported by Weiffenbach and Grossi [1976]. These studies all pertain to two low-orbiting satellites.

In contrast, when techniques originally used for planetary occultation are applied in an analogous manner by using the SST data between a high geostationary satellite in combination with a lower Earth satellite, terrestrial atmospheric refractivity and density data are obtained in an easy and efficient manner. The actual application of this technique for the purpose of weather monitoring was recently realized by Murray and Marini [1976] who used the SST link between ATS-6 and NIMBUS-6 Earth satellites.

2.0 SATELLITE-TO-SATELLITE TRACKING DATA

The SST data is a result of transmitting a phase coherent C-band signal from the ground to ATS-6, where it is translated to S-band frequency and relayed to GEOS-3. GEOS-3 multiplies the received S-band signal by 240/221 and returns it to ATS-6. ATS-6 converts the S-band signal to C-band, and returns it to the ground. The reference frequency of ATS-6 used for the C- to S-band conversion is from a ground transmitted reference. Because of the Doppler motion between ground station and ATS-6, the received reference frequency at ATS-6 is not a constant, thus the ground (ATS-6), (GEOS-3) and return route signal is not strictly phase coherent. The GEOS project call this mode "pseudo coherent."

The received signal at the ground station is heterodyned down to a convenient frequency and the cycles are "N" counted. That is, when N cycles (where N is a pre-selected number) has transpired from initiation of the count, the time at which this event has occurred is recorded to the level of 1 millisecond. Because of this count mechanization, it can be seen that the Doppler averaging time changes directly as the relative distances between ground-ATS-GEOS changes. The data sets we have analyzed so far consisted of 10 second samples of "destruct-count" Doppler.

"Destruct count" Doppler is distinguished from "nondestruct-count" Doppler in the following manner. In the nondestruct-count mode, the number of cycles, N, is measured from a known and fixed time period. The N counts are accumulated from each time period. Thus the phase accumulation (Doppler integration) property inherent in this mode is preserved. The destruct mode does not preserve this property because the time interval is determined by the fixed number of cycles, N. The re-initiation time to begin the next count interval begins on the whole second, therefore, there are time gaps from one count interval to the next and a continuous record of accumulated phase is not possible.

Various synthesizer and frequency multiplier options on-board ATS-6 and at the ground receiver station were supplied [Bryan, Lynn and Hinely, 1975]. This reference also provided us with the format of the data tape which we received from Wallops Station as well as other key information necessary for us to formulate a mathematical model of the SST data.

3.0 DATA ANALYSIS METHODS

The primary measurement is, strictly speaking, a change in the phase path length between the two satellites. If spherical layering is valid locally then the phase path record can be convolved or inverted to a refractivity record. In order to separate the ionospheric effect from the Doppler motion, a computer program (POEAS) removes all relative Doppler motions between the two satellites and the ground station, and properly accounts for the "pseudo-coherent" and "N" count properties of the data. The residuals are first examined for gravitational anomaly effects as well as for poor orbital solution convergence. Various degrees and order of the Earth potential field are used to reduce the residual size. When the orbit is sufficiently converged, it is extrapolated through the atmospheric portion of the data, typically the last five to ten minutes of each pass, where, by the assumption of spherical symmetry in atmospheric density, refractive indices at various altitudes are derived from this data by means of either integral inversion or matching ionospheric parameters by a least square method.

The Earth's atmosphere has considerable asymmetry, especially near the polar regions. Horizontal gradients play a significant role in the deduction of the refractive profile as shown by Grossi and Gay. Under these circumstances, the viewing geometry becomes vital. It was proven by Pirraglia and Gross [1970] that when the angle between the plane of the orbit of the spacecraft (GEOS-3) and the direction of the observation point (ATS-6) are small, then the effects on non-radial (non-spherical) assymmetries become unimportant. The four passes of data we selected satisfy this condition.

Since POEAS is a high precision orbit determination program, all relative station - ATS-6 to GEOS-3 - positions are accurately calculated. Coupled with the ray tracing procedure, accurate evaluations of each individual ray path are performed automatically by the program. Because of these added complexities, detailed analysis to the level of the measurement accuracy is possible, however, the advantage is off-set by heavy and extensive computer

usage. Double iterations are required at each ray calculation. Once to satisfy the equation that relates signal transit time to geometrical distance and second to satisfy the end point conditions of the ray path (i.e., the ray paths must end at the respective spacecraft positions). There are nevertheless several off-setting advantages. The first is to overcome the limitations of the "destruct-count" mode Doppler. Since the analysis includes a ray trace procedure, accurate phase relationships are extrapolated from point to point and compared directly with the data. Further, no assumptions other than spherical structure of the atmosphere are made, and therefore, bending effects are automatically taken into account.

For electron densities N_e on the order of 10^{11} particles per cubic meter, the refractivity, N, is on the order of -1 at S-band signal frequencies. This effect produces a shift in the Doppler frequency of about 1 Hz. The Doppler frequency due to the relative motion of GEOS-3 and ATS-6 is about 40 KHz. The observed data noise is about .05 Hz which yields a 5% accuracy in the ionospheric density measurement.

3.1 Ray Tracing and Adjustments of Ionospheric Parameters by Method of Least Square

The measurement is the change in the phase path length between the two satellites. By assuming that the ray passes through the two satellites in the least time, T, (Fermat's principle) the phase perturbation caused by medium with index of refraction, n, can be computed.

Let

c = speed of light in vacuum
v = speed of light in medium
ϕ = polar angle of the ray path
r = distance of the ray path from geocenter
n = index of refraction = c/v

Consider the situation illustrated in Figure 1. A light ray is required to leave point A, pass through a medium with index of refraction n, and arrive at point B in the least amount of time, T, i.e.,

$$T = \int_S \frac{ds}{v} \tag{1}$$

is to be extremal by finding the proper path S, or

$$T = \frac{1}{c} \int_S nds = \frac{1}{c} \int_S n \sqrt{1 + r^2 \left(\frac{d\phi}{dr}\right)^2}\, dr \tag{2}$$

The path S is determined by finding $\phi = \phi(r)$. A necessary condition for rendering T an extremal is that the integral of (2) satisfy the Euler-Lagrange equation.

$$\frac{\partial F}{\partial \phi} - \frac{d}{dr} \frac{\partial F}{\partial \phi_1} = 1 \tag{3}$$

where

$$\phi_1 = \frac{d\phi}{dr} \tag{4}$$

and

$$F = n(\phi, r) \sqrt{1 + r^2 \phi_1^2} = F(\phi, r, \phi_1) \tag{5}$$

At this point, we note that for the cause where spherical symmetry exists,

$$\frac{\partial F}{\partial \phi_1} = 0 \tag{6}$$

The total bending to infinity can be found as

$$\phi = \int_{r_o}^{\infty} \frac{C}{r\sqrt{n^2 r^2 - C^2}}\, dr \tag{7}$$

where

$$C = r_o\, n_o \cos E_o \tag{8}$$

a. Angular refraction. To evaluate the integral given by (7), make a change of variable to u = rn. It follows that,

$$du = (rn' + n)dr \tag{9}$$

where

$$n' = \frac{dn}{dr} \tag{10}$$

Integration by parts of (7) gives

$$\phi = \frac{\pi}{2} - C \int_{u_o}^{\infty} \left(\frac{rn'}{rn' + n}\right) \frac{du}{u\sqrt{u^2 - C^2}} \tag{11}$$

$$= \frac{\pi}{2} + \delta\phi - E_o \tag{12}$$

We note that $\delta\phi$ will have a singularity whenever u = C and to remove this singularity, transform again the variable u to x by

$$\cos x = \frac{C}{u}\,, \tag{13}$$

yielding for $\delta\phi$,

$$\delta\phi = \int_{x = xo}^{x} \frac{rn'}{(rn' + n)}\, dx \tag{14}$$

b. "Range" or time of flight correction. The path is now known, given by (14) and the transit time, T or R, the measured range is given by

$$R = cT = \int_{r_o}^{\infty} \frac{n^2 r}{\sqrt{n^2 r^2 - C^2}}\, dr \tag{15}$$

Changing variable r to u and integrating (15) by parts as before gives

$$\Delta R = \int_{u_o}^{\infty} - \frac{u}{\sqrt{u^2 - C^2}} \left(\frac{rn'}{rn' + n}\right) du - r_o \sin (E_o - \delta\phi) \tag{16}$$

$$+ r_o n_o \sin E_o$$

The Chapman ionosphere is characterized as

$$Ne - Ne\ (max)\ \exp\ \{\tfrac{1}{2}\ [1 - u - \exp\ (-u)]\} \qquad (17)$$

where

Ne = number of electrons/m^3 at height h
Ne(max) = maximum number of electrons/m^3 occurring at h (max)
h = altitude above Earth
B = scale height and,
u = [h - h (max)]/B

The index of refraction is related to Ne according to electro-magnetic theory by:

$$n = 1 - \tfrac{1}{2}\ \frac{K^2}{f^2}\ Ne = 1 + N \times 10^{-6} \qquad (18)$$

where

N = refractivity
f = transmitter frequency = 2.3×10^9 Hz
K^2 = 80.6 for Ne in units of electrons/m^3

The parameters of the Chapman ionosphere, B, H (max) and Ne (max) are computed by a least square solution from the SST data, and refractivity is computed by (17), and (18).

3.2 Refractivity from Integral Inversion of the SST Occultation Data

Another way to obtain refractivity versus altitude from the SST data is to invert the integral equation relating the phase perturbations with the refractivity. If it is assumed that the ray paths are straight lines passing through a spherically symmetric atmosphere then the inversion is accomplished by using a method described by Fjeldbo and Eshleman [1968]. This method was

used successfully to deduce the Martian ionospheric refractivity. This method to find refractivity versus height by means of integral inversion procedure is as follows. The last 5 minutes of the SST data were first de-trended by a low order least square polynomial fit to the data, to remove small biases and drifts.

Since the SST data was destruct-count Doppler, phase residuals were created by numerically integrating the Doppler residuals using the trapezoidal rule. A program generated the geocentric positions of ATS-6 and GEOS-3, the initial conditions of the orbits being supplied by the POEAS converged orbits. The relative geometry between ATS-6 and GEOS-3 were computed and minimum geocentric ray distance for each data point was calculated. The assumption is that ray bending can be neglected. (This assumption is justified here because the density of the Earth's ionosphere is small and thus bending effects are negligible.) On this basis (1) of Section 3.1 can be modified as

$$R = \int_S ds + \int_S (N \times 10^{-6}) ds \tag{19}$$

where S is now the straight line path connecting the two satellites.

The ray path perturbation, ΔR, is represented by the last term in (19) and is approximated by a system of K linear equations of the form

$$\Delta R(m) = N(m)\ \Delta S(m,m) + 2 \sum_{n=1}^{m-1} N(n)\ \Delta S(m,n), \tag{20}$$

for the mth ray, where N(n) is the refractivity in the nth layer. The element $\Delta S(m,n)$ designates the length of that portion of the mth ray which lies within the nth layer.

Upon occultation, the first ray (data point) passes through the topmost layer, and the refractivity (assumed constant in this spherical shell) is calculated. The next ray passes through the topmost shell and the next shell below it. The refractivity is calculated for that shell. Layer by layer,

the refractivity (constant for each consecutive shell) is calculated until the last layer (the lower-most) is encountered. In this manner the entire atmosphere refractivity profile is obtained. It was assumed in this procedure that ray-bending is negligible and therefore this type of analysis is permissible. Further, numerical integration of destruct-count Doppler may introduce sizable truncation error in the subsequently created phase measurements. Both of these considerations present potential problems in finding the refractivity profile from the destruct-count Doppler. To assure ourselves that the assumptions did not seriously damage or invalidate the analysis, a simulation was performed. Artificial destruct-count Doppler were created by using the ray trace method of Section 3.1, which accounted for all ray-bending and layering effects. These data had the appropriate orbital geometry and atmospheric distortion properties. A profile inversion was performed on this data and the results recovered the atmosphere to better than 90 percent.

4.0 RESULTS

Four passes of data were analyzed. Two of the passes were south-bound and ended in occultations over the south polar region. The other two were north-bound. One occulted over the Aleutian Islands, and the other occulted west of the Hawaiian Islands.

The occultation aspects as seen from ATS-6 are shown in Figure 2. The solid square represents the limb and the sinusoidal curves are the ground traces of GEOS-3 for the four passes of data. The numbers of 169, 232, 239, 259 represent the GEOS-3 revolution numbers. The occultations always occur on the limb and are indicated by the triangles. Table 1 lists the date, time, longitude and latitude by the revolution numbers.

Figure 3 shows typical SST Doppler residuals (i.e., data minus estimated data) after orbit adjustments of GEOS-3 and ATS-6. Perturbations from the Moon and Sun and a 15th order/degree Earth gravity field were included in the orbit solution. Neglect of the solar radiation pressure perturbation on ATS-6 caused a sinusoidal fluctuation of 0.05 Hz [T. V. Martin, et. al., 1976]. The SST data quality was excellent and exhibited data noise of about 0.01 Hz for a Doppler integration time of about 6.5 seconds. When the data was extended to include the remaining 5 minutes of the pass when GEOS-3 was setting behind the Earth, a definite atmospheric signature of 1.5 Hz appeared at the end of the pass (Figure 4). Every data set examined showed a similar signature. Some data residuals were as large as 3 to 5 Hz, as compared to the random noise of 0.01 Hz. Thus the atmospheric affects in the data were very strong and, therefore, presented no trouble in deducing refractivity. The atmosphere sensing began at an altitude of 700 km and ended at an altitude of 40 km, thereby traversing completely through the ionosphere and partially through the neutral atmosphere.

Parameters of a Chapman model ionosphere were matched to the atmospherically distorted portion of the SST data so that the Doppler residuals were minimized in a least square sense. For each data point, POEAS calculated the minimum height of the ray path, taking into account the respective

motions of the ground station, ATS-6 and GEOS-3. The result of this least square adjustment is shown in Figure 5 where it can be seen that the Doppler residuals have been reduced from 1.5 Hz to 0.25 Hz. The ordinate of Figure 5 has been changed from time to the radius of minimum height of the ray. The Chapman model which gave this residual profile is shown in Table 2.

As an alternate to parameter fitting, an integral inversion method described in Section 3.2 was adapted here for purpose of comparison. A systematic difference can be seen in Figure 6. This discrepancy is the result of a numerical integration of destruct-count Doppler data containing systematic errors of 0.05 Hz. Artificially created error-free data gave good agreement between the ray-trace and integral inversion methods.

The remaining three passes for GEOS (Revolutions 232, 239, and 259) were analyzed by inverting the SST data. Model matching was not attempted since this method required considerable computer expense. The data points are spaced at altitude intervals of 30 kilometers, which resulted from taking Doppler data at a 10 second rate and GEOS-3 setting at a rate of 3 km/sec relative to ATS-6. Figures 7 and 8 are plots of refractivity vs the minimum geocentric distance of the ray paths. In the absence of magnetic fields, electron density, Ne, is proportional to refractivity N, at S-band, by

$$Ne(\#/m^3) = -.15 \times 10^{12} N \qquad (21)$$

To convert geocentric radii to altitude it is necessary to define a reference surface. Since the reduction was made without reference to a surface, but to the distance from the geocenter, the plots were left in terms of geocentric radii.

In Figure 7, refractivity over the south pole is plotted every 10 seconds. The F layer appears more diffuse in Rev 169 than Rev 239. In Rev 239 the F layer shows a maximum refractivity at 6600 km, and quickly drops and merges into neutral atmosphere. Since the data were taken at ten second intervals, little information about the troposphere can be gained. The final points of Passes 169 and 239 show an upswing and a positive refractivity due to the troposphere.

Table 1. Time and Locations of Occultations

Rev. No.	GMT of Occultation	Long (deg)	Lat (deg)
169	4/21/75 23:17	162° W	67° S
232	4/26/75 9:20	168° W	55° N
239	4/26/75 22:08	167° W	59° S
259	4/28/75 7:21	174° W	27° N

Table 2. Chapman Ionosphere Parameters for Rev. No. 169
April 21, 1975 23:17 GMT

Max. Electron Density (No./m^3)	$(0.1453 \pm 0.0028) \times 10^{12}$
Scale Height (km)	65.51 ± 0.72
Height of Max. Electron Density (km)	237.49 ± 2.02

Figure 8 shows a plot of refractivity over the Northern Hemisphere. Revolution 259 is the most equatorial of all the data received and exhibits a pronounced main F layer.

Another pass, which occulted over the north polar region was also analyzed (Revolution 232). This pass of data showed the effect of a poor orbit solution where the entire profile was skewed. Examination of the orbit solution for Rev 232 revealed a poor adjustment in the GEOS-3 mean anomaly probably due to the unfavorable geometrical aspect of this pass relative to ATS-6. It should be mentioned that SST data alone tends to yield weak orbit solutions and many orbits, which were used for gravity analysis only, were slow or difficult to converge. One such case was Rev 232 and, although the general atmospheric structure appears undistorted and informative, it is necessary to re-establish the GEOS-3 orbit for this pass.

ACKNOWLEDGEMENTS

It is a pleasure to express my deep appreciation to Mr. D. Cain and Dr. Mario Grossi for their thoughtful assistance and encouragement throughout this investigation. Special thanks are given to Mr. P. A. Laing, for all his work in the modification of POEAS and to Mssrs. W. S. Sjogren and R. N. Wimberley for their initial preparation of the data. I am grateful to Mr. H. R. Stanley, GEOS-3 Project Scientist, of Wallops Station and to Messrs. I. M. Salzberg and B. J. Trudell (Goddard Space Flight Center) for the coordination and the collection of this unique and interesting SST data.

5. REFERENCES

Bryan, J.W., J. J. Lynn, and A. O. Hineley (1975), A User's Guide for Satellite to Satellite System Observations and Data Formats, Goddard Space Flight Center, NASA/GSFC, Greenbelt, MD.

Fjeldbo, G., and V. R. Eshleman (1968), The Atmosphere of Mars Analyzed by Integral Inversion of the Marine IV Occultation Data, Planetary Space Science, 16 pp. 1035-1059.

Grossi, M. D., and R. H. Gay (1975), Doppler Measurements of the Ionosphere on the Occasion of the Apollo-Soyuz Test Project, Smithsonian Special Report 366 and 367, Smithsonian Astrophysical Observatory, Cambridge, MA.

Kliore, A., D. Cain, G. S. Levy, V. R. Eshleman, G. Fjeldbo, and F. Drake (1965), Occultation Experiment: Results of the First Direction Measurement of Mars' Atmosphere and Ionosphere, Science, 149 No. 3689, pp. 1243-1248.

Kliore, A. (1969), Some Remarks on Meteorological Measurements with Occultation Satellites, Space Research 9, North Holland Publishers.

Martin, T.V., I. H. Oh, J. A. Kogut, W. F. Eddy, C. F. Martin, T. J. Grenchik, and J. A. Behuncik (1976), An Evaluation of TDRSS Using ATS-6/GEOS-3 Satellite-to-Satellite Data, EOS Transactions AGU 57, No. 12.

Morrison, A.R., S. Ungar, and B. B. Lusignan (1972), An Occultation Satellite System for Determining Pressure Levels in the Atmosphere, NASA CR-132436, Stanford University, Stanford, CA.

Murray, C.W., and J. W. Marini (1976), Atmospheric Pressure and Temperature Distributions Recovered from ATS-6/NIMBUS-6 Radio Occultation Data, EOS Transactions AGU 57, No. 12.

Pirraglia, J., and S. H. Gross (1970), Latitudinal and Longitudinal Variation of a Planetary Atmosphere and the Occultation Experiment, Planetary Space Science, 18, pp. 1769-1786.

Weiffenbach, C.G. and M. D. Grossi (1976), Doppler Tracking Experiment MA-089, Apollo-Soyuz Test Project Preliminary Science Report, NASA TMX-58173, U. S. Government Printing Office, Washington, D. C.

LIST OF FIGURES

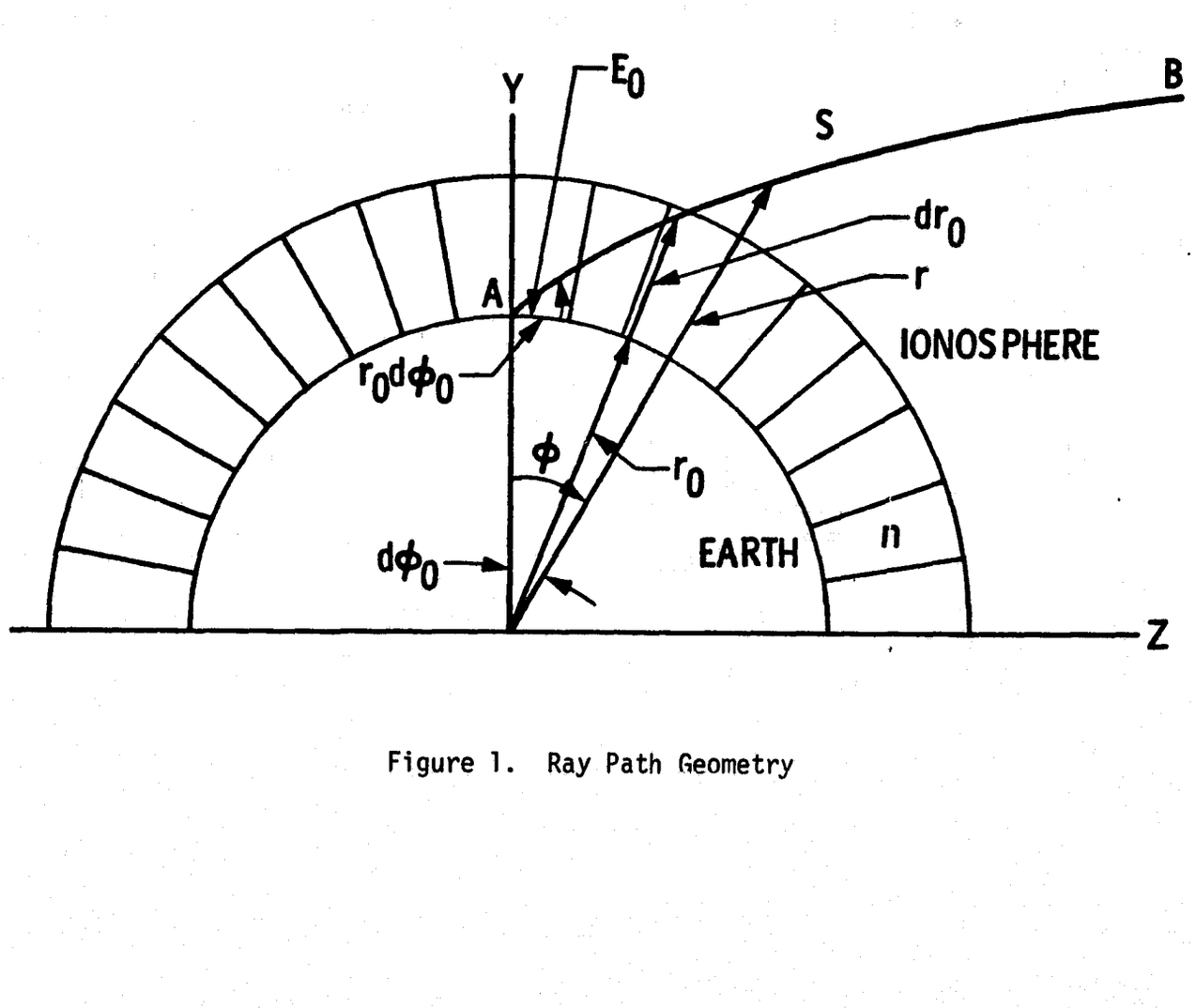

Figure 1. Ray Path Geometry

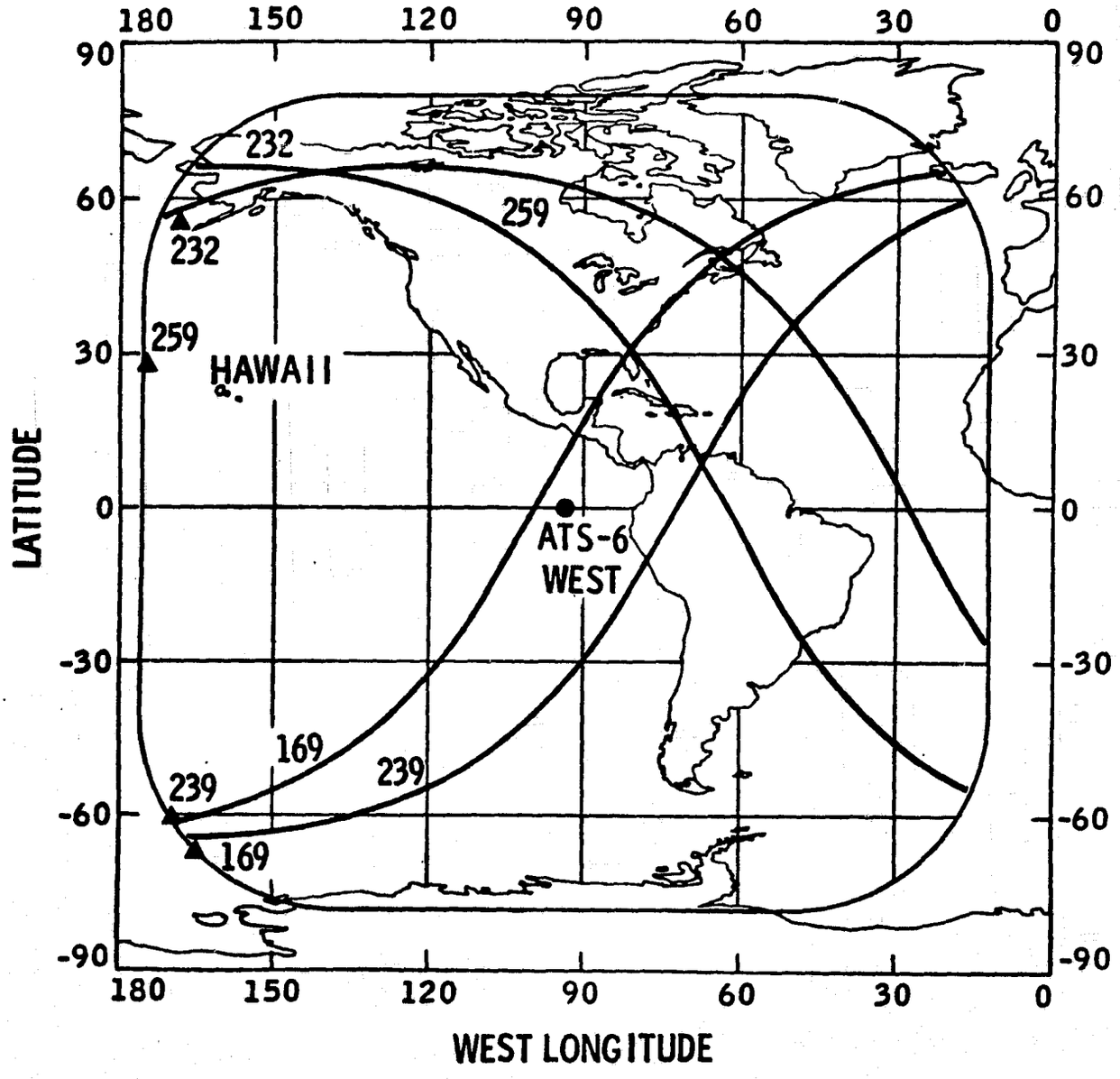
180
150
120
90
60
30
0
90
60
30
0
-30
-60
-90
232
259
169
239
HAWAII
ATS-6
WEST
LATITUDE
WEST LONGITUDE
▲OCCULTATION LOCATION

Figure 2

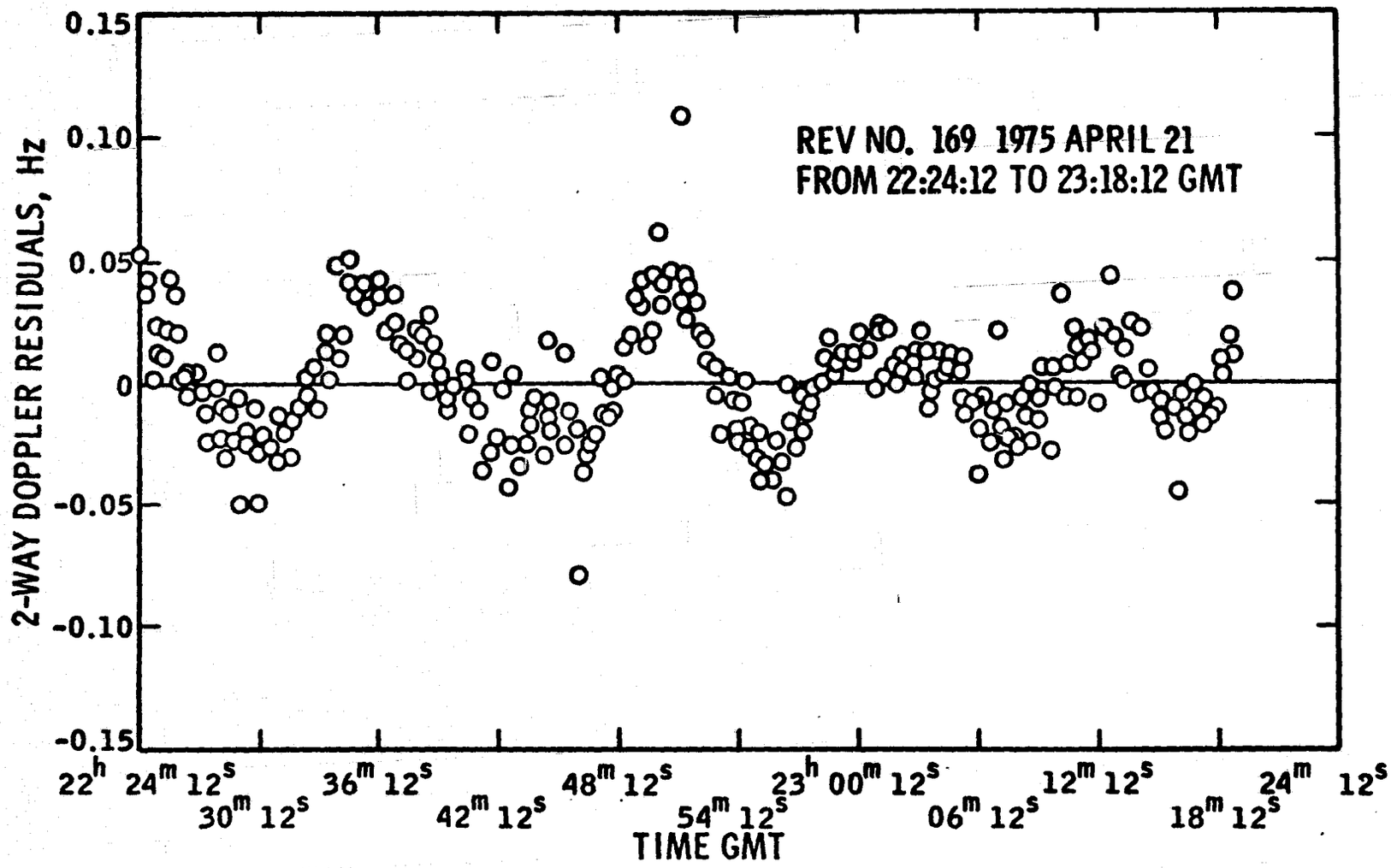
REV NO. 169 1975 APRIL 21
FROM 22:24:12 TO 23:18:12 GMT
2-WAY DOPPLER RESIDUALS, Hz
0.15
0.10
0.05
0
-0.05
-0.10
-0.15
22h 24m 12s
30m 12s
36m 12s
42m 12s
48m 12s
54m 12s
23h 00m 12s
06m 12s
12m 12s
18m 12s
24m 12s
TIME GMT

Figure 3

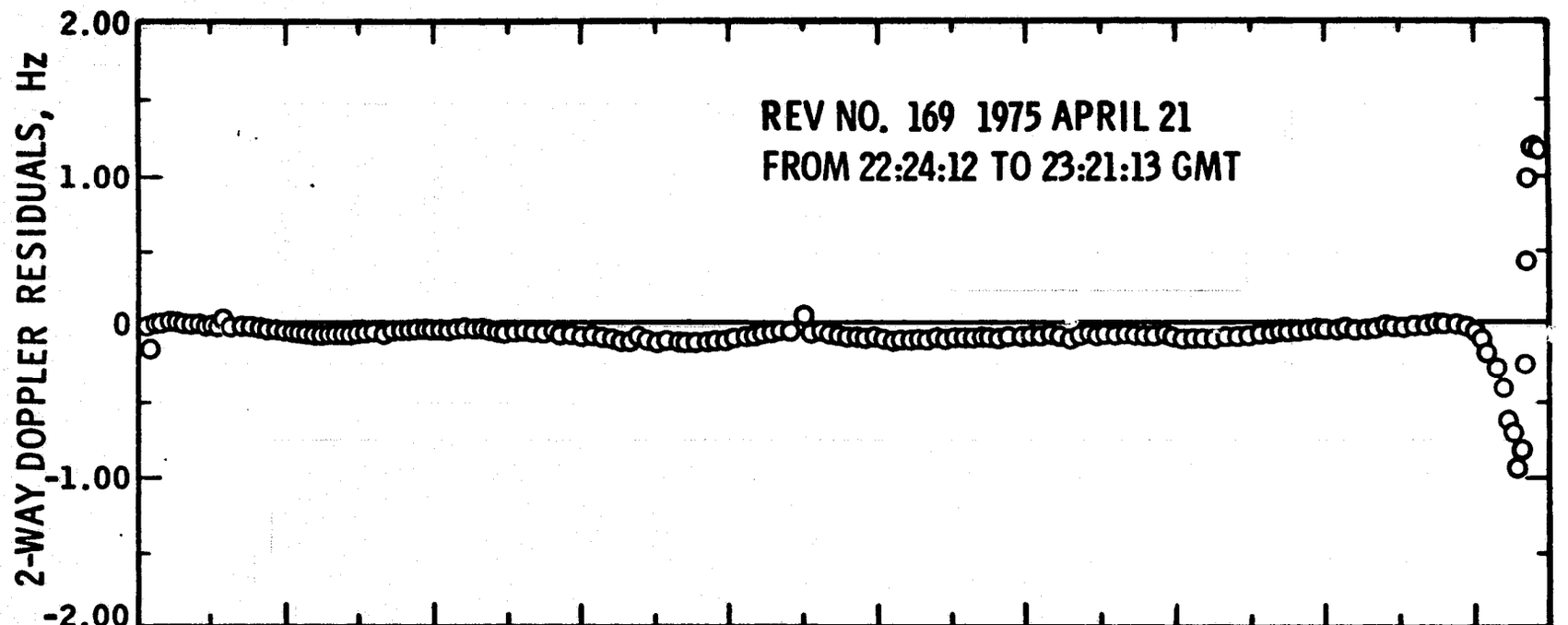
REV NO. 169 1975 APRIL 21
FROM 22:24:12 TO 23:21:13 GMT
2-WAY DOPPLER RESIDUALS, Hz
2.00
1.00
0
-1.00
-2.00
22hr 24m 12s
30m 12s
36m 12s
42m 12s
48m 12s
54m 12s
23hr 00m 12sec
06m 12s
12m 12s
18m 12s
22m 12s
TIME (GMT)

Figure 4

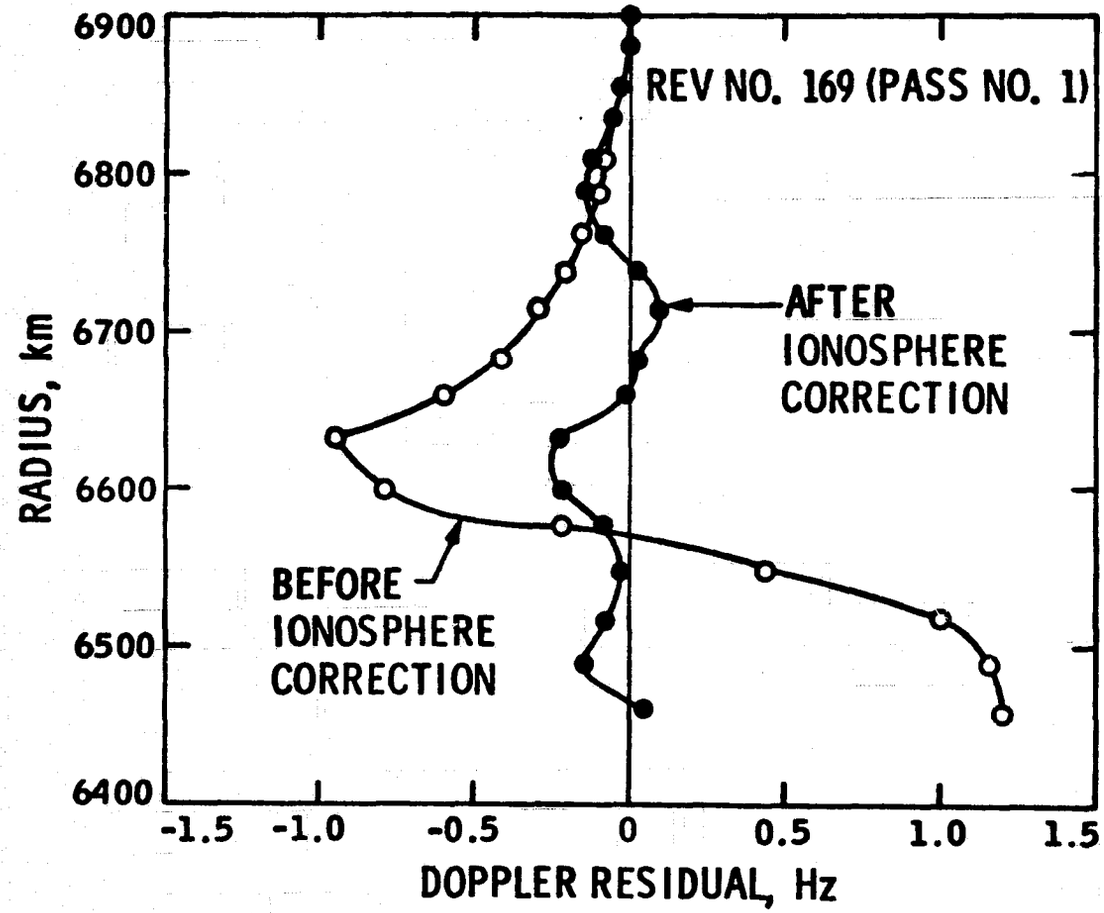
REV NO. 169 (PASS NO. 1)
AFTER
IONOSPHERE
CORRECTION
BEFORE
IONOSPHERE
CORRECTION
RADIUS, km
6900
6800
6700
6600
6500
6400
-1.5
-1.0
-0.5
0
0.5
1.0
1.5
DOPPLER RESIDUAL, Hz

Figure 5

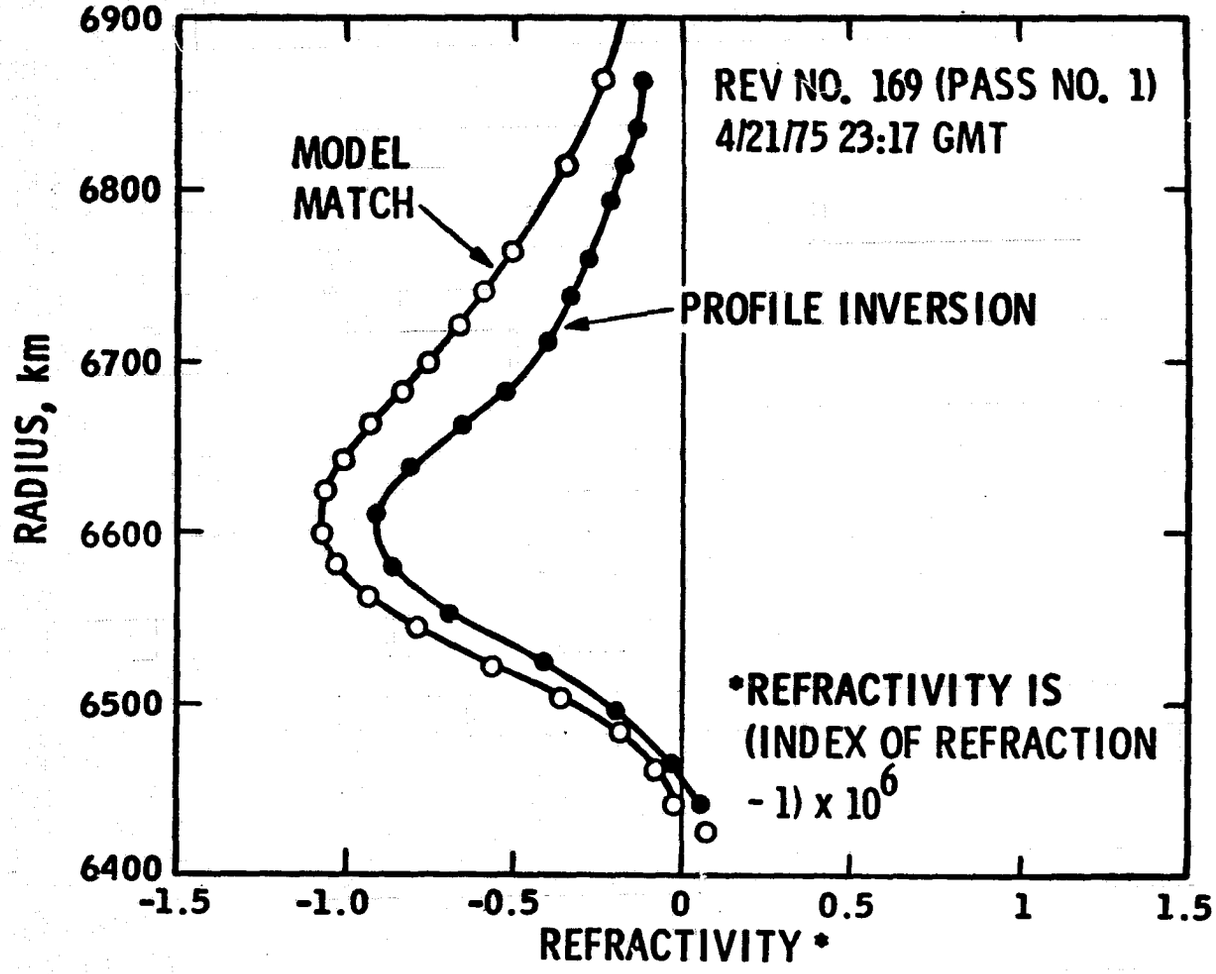
6900
6800
6700
6600
6500
6400
RADIUS, km
-1.5
-1.0
-0.5
0
0.5
1
1.5
REFRACTIVITY *
REV NO. 169 (PASS NO. 1)
4/21/75 23:17 GMT
MODEL
MATCH
PROFILE INVERSION
*REFRACTIVITY IS
(INDEX OF REFRACTION
- 1) x 10^6

Figure 6

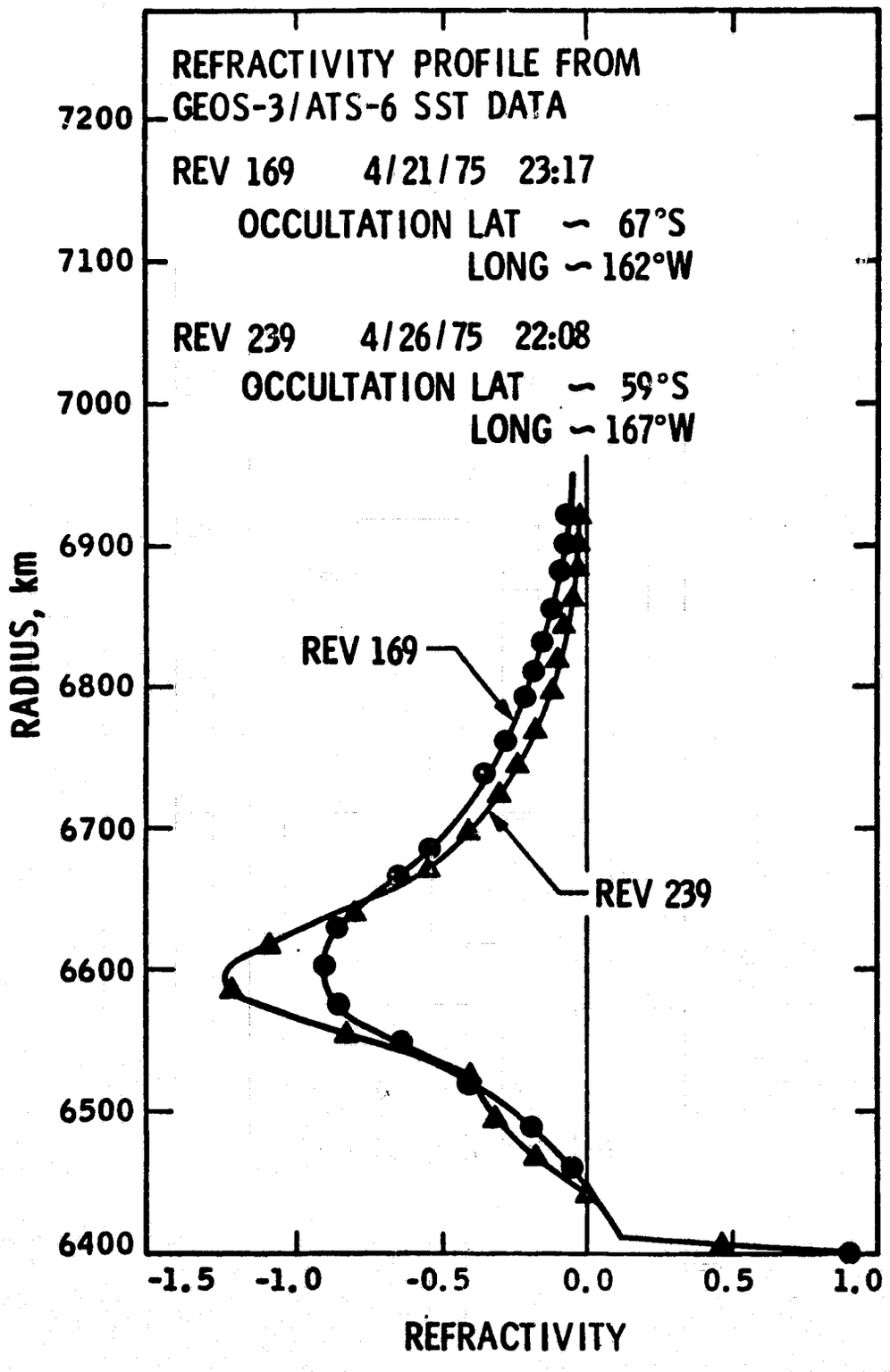
REFRACTIVITY PROFILE FROM
GEOS-3/ATS-6 SST DATA
REV 169 4/21/75 23:17
OCCULTATION LAT ~ 67°S
LONG ~ 162°W
REV 239 4/26/75 22:08
OCCULTATION LAT ~ 59°S
LONG ~ 167°W
REV 169
REV 239
RADIUS, km
7200
7100
7000
6900
6800
6700
6600
6500
6400
-1.5
-1.0
-0.5
0.0
0.5
1.0
REFRACTIVITY

Figure 7

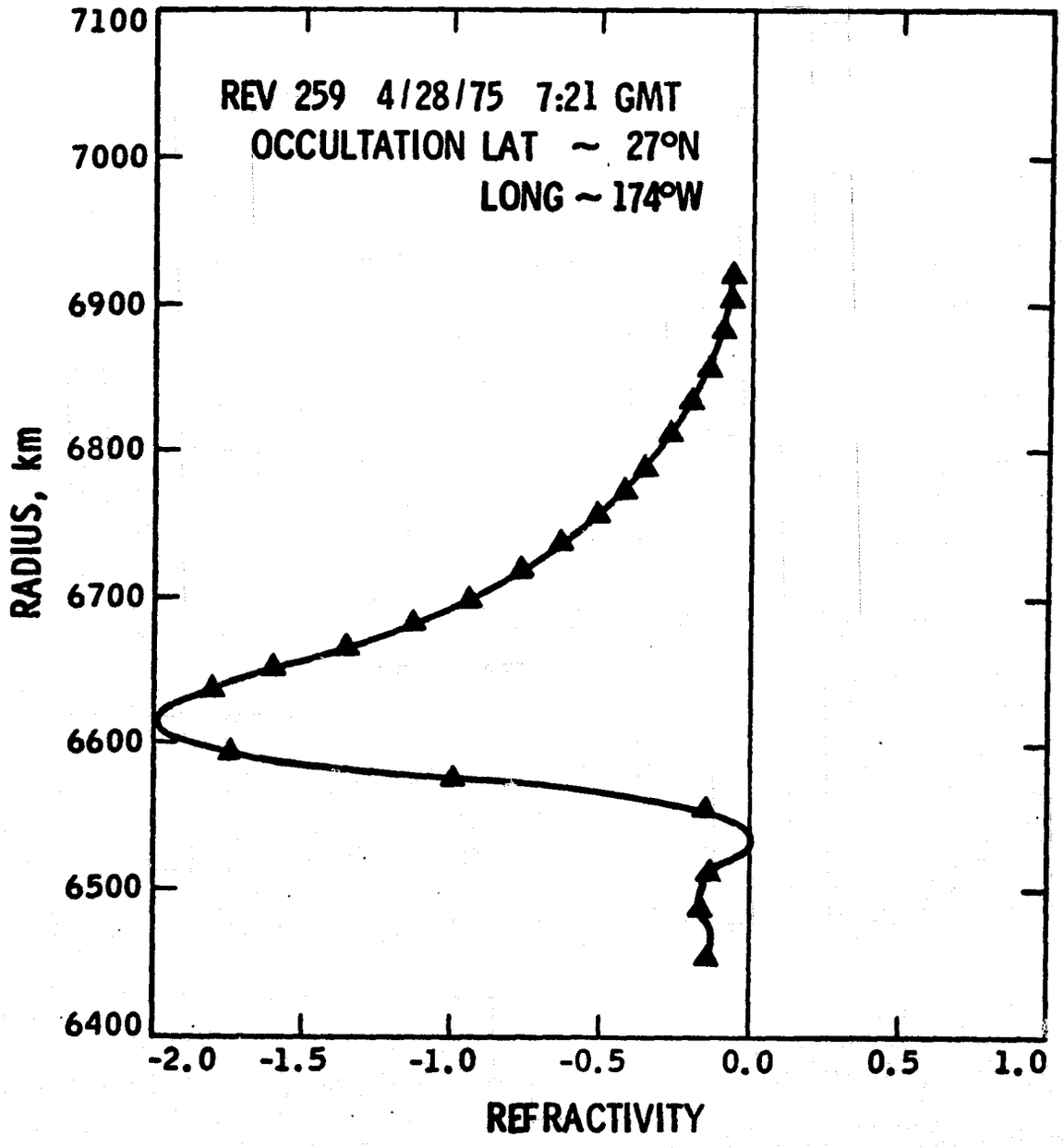
REV 259 4/28/75 7:21 GMT
OCCULTATION LAT ~ 27°N
LONG ~ 174°W
RADIUS, km
7100
7000
6900
6800
6700
6600
6500
6400
-2.0
-1.5
-1.0
-0.5
0.0
0.5
1.0
REFRACTIVITY

Figure 8